NEUROSCIENCE

Functional anatomy of the subthalamic nucleus and the pathophysiology of cardinal features of Parkinson's disease unraveled by focused ultrasound ablation

Rafael Rodriguez-Rojas[1,2,3,4]†, Jorge U. Máñez-Miró[1,5]†, José A. Pineda-Pardo[1,3,4], Marta del Álamo[1], Raúl Martínez-Fernández[1,3,4], José A. Obeso[1,3,4,6]*

The subthalamic nucleus (STN) modulates basal ganglia output and plays a fundamental role in the pathophysiology of Parkinson's disease (PD). Blockade/ablation of the STN improves motor signs in PD. We assessed the topography of focused ultrasound subthalamotomy (n = 39) by voxel-based lesion-symptom mapping to identify statistically validated brain voxels with the optimal effect against each cardinal feature and their respective cortical connectivity patterns by diffusion-weighted tractography. Bradykinesia and rigidity amelioration were associated with ablation of the rostral motor STN subregion connected to the supplementary motor and premotor cortices, whereas antitremor effect was explained by lesioning the posterolateral STN projection to the primary motor cortex. These findings were corroborated prospectively in another PD cohort (n = 12). This work concurs with recent deep brain stimulation findings that suggest different corticosubthalamic circuits underlying each PD cardinal feature. Our results provide sound evidence in humans of segregated anatomy of subthalamic-cortical connections and their distinct role in PD pathophysiology and normal motor control.

INTRODUCTION

The subthalamic nucleus (STN) via its glutamatergic efferent projections exerts a major excitatory influence on neuronal output activity of the basal ganglia. It plays a pivotal role in basal ganglia pathophysiology and is the favored neurosurgical target for functional interventions in patients with Parkinson's disease (PD) worldwide (*1*, *2*). According to its functional organization, the STN is divided into motor, associative, and limbic regions, which are anatomically parcellated rostrocaudally and mediolaterally (*3*). Admittedly, this subdivision is not entirely well established and accepted (*4*) as the boundaries are not strictly limited and functions also overlap somewhat. On the other hand, the classic functional tripartite organization of the STN and basal ganglia has been documented in nonhuman primates and patients (*5*–*7*). Moreover, and specifically with regard to the current study, there are no major doubts about the dorsolateral STN region being essentially motor and highly involved in the pathophysiology of movement disorders. Physiological and trace labeling experiments in monkeys have shown that the motor STN subregion is located caudally and dorsolaterally, and it is further subdivided mediolaterally and rostrocaudally into the supplementary motor area (SMA) and primary motor cortex (M1) cortical representations (*5*, *6*). More recently, this dual somatotopic representation of M1 and SMA cortical projections within the motor STN has been shown in a diffusion-weighted imaging/functional magnetic resonance imaging (MRI) study in controls and patients with PD (*7*).

Historically, the dopaminergic striatal deficit and associated clinical manifestations of PD have been considered to be one fundamental piece of evidence for the primary role of the basal ganglia in motor control (*8*–*10*). Accordingly, motor signs of PD can be assessed as indicators of derangement of normal aspects of motor behavior. Expanding on that, a mechanistic study of cardinal features of PD could further the understanding of the functional anatomy of corticobasal ganglia circuits and the STN in particular, along with its role in control of movement.

In the mid-twentieth century, astute observations stemming from neurosurgical procedures pointed out that lesion location for improving rigidity versus tremor had different topography within the thalamus and globus pallidus (*11*–*13*). More recently, in the era of deep brain stimulation (DBS), there have been several studies that describe the most effective therapeutic sites (i.e., sweet spots) for PD with STN-DBS (*13*). Although these studies were generally based on a small number of patients, the notion emerged that different electrode locations differentially improved motor features of PD (*14*–*17*). Very recently, a major neuroimaging study in a large cohort (n = 129) of patients with PD who underwent bilateral STN-DBS carried out a data-driven analysis to identify the stimulated tracts related to the optimal clinical outcomes for each cardinal motor manifestation (*18*). Thus, STN-DBS of the posterior STN and surrounding tracts connected to the M1 and the cerebellum correlated with better tremor outcome, whereas the best effect against bradykinesia and rigidity was related to electrodes stimulating the anterior STN projections to premotor and supplementary cortices. Notably, another projection to the brainstem was revealed to be relevant for improvement in axial signs (*18*). This previously unidentified pathway fits with previous experience in PD whereby the response to medication (i.e., levodopa and dopaminergic drugs) is more evident against bradykinesia and rigidity than tremor, but the opposite has generally been the case in response to functional neurosurgery (ablation and DBS) (*19*). The underlying pathophysiological basis for such differences in response to dopaminergic drugs and surgery had never been fully understood, but the current evidence (*18*, *20*) suggests the existence of segregated corticobasal

[1]HM CINAC (Centro Integral de Neurociencias Abarca Campal), Hospital Universitario HM Puerta del Sur, HM Hospitales, Madrid, Spain. [2]Facultad de Tecnología y Ciencia, Universidad Camilo José Cela, Madrid, Spain. [3]Instituto de Investigación Sanitaria HM Hospitales, Madrid, Spain. [4]CIBERNED, Instituto de Salud Carlos III, Madrid, Spain. [5]PhD Program in Neuroscience, Autónoma de Madrid University-Cajal Institute, Madrid, Spain. [6]Medical School, CEU-San Pablo University, Madrid, Spain.
*Corresponding author. Email: jobeso.hmcinac@hmhospitales.com
†These authors contributed equally to this work.

ganglia connections that possibly explain the differences and variability in response to treatments.

Here, we describe a hypothesis-driven analysis aiming to define the functional anatomy of the STN and its cortical connectivity by using a classic approach of experimental neurology, i.e., the impact of focal ablation. We applied currently available neuroimaging to ascertain how different lesion locations within the STN have a distinct impact on motor features of PD unilaterally. Thus, unlike DBS, generally a bilateral procedure, which stimulates a relatively large volume of tissue locally and may spread to surrounding neural structures and projections (*21*), a focal unilateral ablation has a very immediate clinical effect by blocking a specific subregion of the targeted nucleus (*22*, *23*). In this study, we assessed in detail the topography of focused ultrasound subthalamotomy (FUS-STN) and identified statistically validated brain voxels where the presence of a lesion affected the severity of each motor feature using voxel-based lesion-symptom mapping (*24*). Moreover, by combining morphometry and diffusion-weighted tractography, we defined the cortico-subthalamic connectivity patterns related to the optimal benefit against tremor, rigidity, and bradykinesia, respectively. These results unravel a tight association between segregated topography within the STN and cortical motor areas on the one hand and specific PD motor signs on the other. Accordingly, we here establish a near to causal relationship between the anatomical organization of the STN-cortical connections and the origin of tremor, bradykinesia, and rigidity. In turn, the pathophysiological findings are used to discuss the putative role of the STN and basal ganglia circuits in the control of normal movement.

RESULTS

Clinical and methodological approach: A summary

A topographic analysis of subthalamic lesions was made in a cohort of 51 patients with PD treated in our center with FUS-STN. The initial group of patients ($N = 39$, referred here as the Test Cohort) was participants in a pilot open-label study or in a randomized sham-controlled trial, which provided class I evidence on the safety and efficacy of unilateral FUS-STN for the treatment of PD (fig. S1) (*25*, *26*). Adverse events were transient and mild in most instances. Hemichorea-hemiballism secondary to subthalamotomy was not a main side effect and is not further considered here.

In the 24-hour posttreatment MRI, lesions had a mean (SD) volume overlap of 53 ($\pm$ 23) mm^3 within the STN, mainly encroaching on the posterolateral motor STN region (fig. S2). The lesions were consistently and reproducibly identifiable (mean inter-rater kappa = 0.87 $\pm$ 0.05). Lesion size, location, and the corresponding motor improvement of each cardinal motor feature were somewhat variable, which makes possible the current correlational analysis. Five patients who did not exhibit resting tremor at baseline were excluded from the tremor-related analysis ($n = 34$). Specific data on the topography of the lesions and the clinical outcome for every subject are given in tables S1 and S2.

Upon completion of the initial study and analysis, another pilot study was carried out in 12 patients with PD with less than 5 years of evolution since diagnosis with the aim of assessing the viability and safety of subthalamotomy in a non-advanced population (*27*). This group is referred to here as the Validation Cohort because results from the initial Test Cohort were used to improve STN targeting. This allowed to test prospectively the value and predictability of the main findings described below.

Probabilistic lesion maps of efficacy for each cardinal feature

First, we determined the location of the focal ablation within the STN associated with maximal clinical improvement for a given motor sign. Thus, probabilistic lesion maps voxel weighted by the corresponding clinical improvement were independently generated for bradykinesia, rigidity, and tremor. Sign-related mean effect maps (i.e., mean image) according to the outcomes on each cardinal feature are shown in Fig. 1 (left columns) along with the respective *P*-images (Fig. 1, right columns) displaying only those voxels that contributed with statistical significance ($P < 0.05$; Brunner-Munzel test) to the clinical improvement for every cardinal motor feature (see Materials and Methods for details). Together, a better antibradykinesia effect was associated with lesioning the anterior area of the motor STN as shown in Fig. 1 (upper row). Conversely, the effect of the ablation on tremor showed an anterior-posterior gradient (Fig. 1, bottom row), indicating greater improvement as the ablation affected mainly within the foremost posterolateral region of the motor STN. Of note, the voxels related with the greater antirigidity effect (Fig. 1, middle row) were located between those voxels optimal for bradykinesia and tremor amelioration, respectively.

STN functional anatomy unraveled by the relationship between lesion location and motor improvement

The topography of the focal ablation responsible for optimal benefit on cardinal motor feature (i.e., sweet spot) was obtained from the probabilistic sign-related lesion maps (Fig. 2). After transformation onto the standard Montreal Neurological Institute (MNI) space (MNI152-NLIN2009 version), these sweet spots were registered to a connectivity-based STN atlas segmented in four functional regions according to related connectivity to primary motor, supplementary motor, associative, and limbic cortices (Fig. 2, left column) (*7*). The center of mass of the sweet spots (MNI coordinates) for alleviating bradykinesia ($x/y/z = -11.4/-14.0/-6.9$) and rigidity ($x/y/z = -13.4/-14.4/-6.7$) was located anterior, medial, and inferior within the SMA representation, while the tremor-effective optimal target was located more posterior-laterally and superior within the M1 portion ($x/y/z = -14.2/-17.3/-6.6$) (Fig. 2, right columns). Consistently, these clinically effective sweet spots showed a distributed topography (Fig. 2, A to C). The optimal lesion topography associated with net improvement in bradykinesia largely coincided (76.7% of the sweet spot volume) with the SMA-connected subregion, thus more anterior and medial within the motor STN, with less impact on M1 and associative subregions (15.8 and 7.5%, respectively). Conversely, the best antitremor lesion mainly covered the M1 (posterior and lateral) corresponding subregion (67.7% of the sweet spot volume), albeit with some degree of extension of the lesion onto the SMA-connected subregion (32.3%). The sweet spot for benefit against rigidity was located between these two previously described subregions, not only affecting more prominently the SMA-STN (72.4%) but also encroaching on M1-STN (26.4%). The extension of these sweet spots did not substantially reach the most anterior-medial region of the STN corresponding to the associative and limbic circuits (table S1). Accordingly, the distribution of sweet spots allows us to envision a relationship between the impact of the lesion within specific STN motor subregions and the improvement of each cardinal feature.

Predictor model of motor outcome after focal STN ablation

A predictor model for clinical improvement of FUS-STN was developed by using a multiple regression analysis to further account

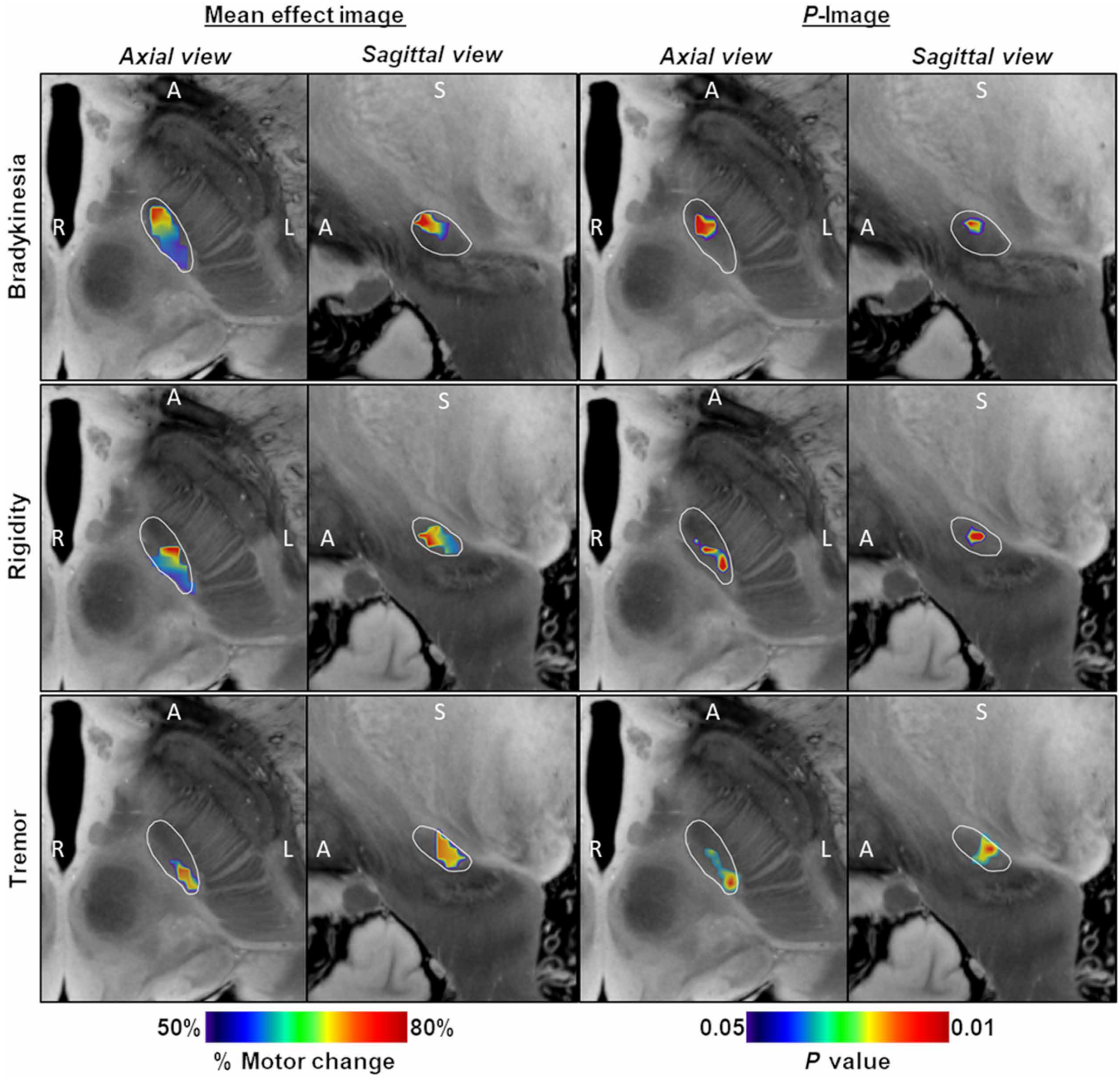

Fig. 1. Probabilistic FUS-STN lesion location maps associated with improvement in cardinal motor features. (**Left**) Axial and sagittal slices of the mean effect image for each motor feature, color coded by the degree of improvement. (**Right**) Corresponding *P*-images. Color coding depicts the results of Brunner-Munzel test on a voxel-by-voxel basis. Only voxels that survived a $P < 0.05$ permutation threshold are included. The STN, outlined in white, is superimposed on slices of a 100-μm, 7-T brain scan in the MNI152 space (*76*). The image orientation is indicated for each slice: A, anterior; S, superior; and R/L, right/left.

for the relationship between lesion topography and the functional anatomy of the STN. These included the lesion volume within the STN subregions (i.e., $V_{\text{SMA-STN}}$, $V_{\text{M1-STN}}$, $V_{\text{ASSOC-STN}}$, and $V_{\text{LIMBIC-STN}}$), defined by a connectivity-based atlas (*7*), as the main contributing factors (i.e., independent variables) to motor outcome (Fig. 3), and it was further adjusted for total lesion volume. According to the model, greater improvement in bradykinesia is achieved by lesions with a larger impact within the SMA-STN motor subregion ($\beta = 0.658$; $P < 0.001$). Conversely, the more the lesion affects within the M1-STN motor subregion, the larger is the associated tremor effect ($\beta = 0.577$; $P = 0.001$). The reduction in contralateral rigidity is also significantly correlated with the volume of the SMA-STN subregion ablation ($\beta = 0.439$; $P = 0.005$). Of note, no statistically significant association of the impact on associative and limbic subregions with motor outcome could be detected (table S2).

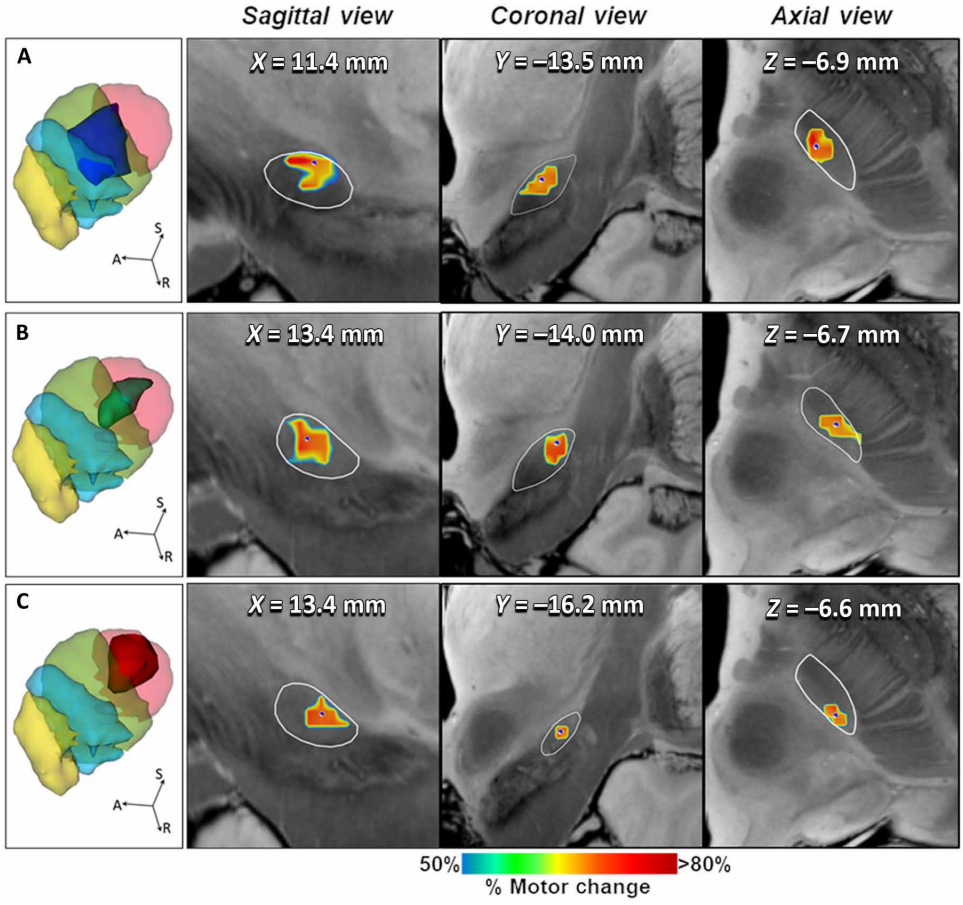

Fig. 2. Topography of FUS-STN lesions for best clinical effect on cardinal motor features. Left column illustrates three-dimensional (3D) rendering of significant mean effect image (i.e., sweet spot) for (**A**) bradykinesia (dark blue surface), (**B**) rigidity (green surface), and (**C**) tremor (red surface), superimposed to a 3D representation of the quadripartite STN atlas (*7*). Functional subregions of the STN are highlighted (primary sensorimotor in red, supplementary motor in green, associative in blue, and limbic in yellow). The following columns show the sagittal, coronal, and axial views of significant mean effect image, color coded by the degree of improvement for each clinical feature relative to STN anatomy (white outlines) and overlaid with an ultrahigh-resolution (100-μm) template of the human brain (*76*). Colored voxels survived a *P* threshold of 0.05 (Brunner-Munzel rank test), after permutation-based FDR correction for multiple comparisons. The MNI coordinates in the sagittal, coronal, and axial planes of the center of mass (blue dot) of each sweet spot are also represented. A, anterior; S, superior; R, right.

Corticosubthalamic connectivity patterns underlying cardinal motor features

We calculated the connectivity model seeded on the clinically effective sweet spots and corresponding projections to cortical areas defined by a human motor area template (Fig. 4) (*28*). This connectivity analysis confirmed that the STN zone associated with best improvement in bradykinesia is mainly connected to the SMA, pre-SMA, and dorsal premotor cortex (PMd) (Fig. 4A). Regarding rigidity, voxels displaying the optimal ablation effect showed relevant projections to both SMA and PMd and, to a lesser extent, to pre-SMA and M1 (Fig. 4B). Conversely, the best effect against parkinsonian tremor was related to the impact within an STN area with a major projection to the M1, although a less notable impact on the connections to the ventral premotor cortex (PMv) and SMA is also present (Fig. 4C). The connectogram (Fig. 4D) confirms that sweet spots for each cardinal feature showed different and segregated cortical connectivity patterns. These results from the connectivity analysis were consistent with the quantitative approach provided by the multiple regression model (Fig. 3).

Validation of results in a prospective cohort

The above-described results led us to validate the findings prospectively in an out-of-sample cohort in whom lesions were planned according to our current lesion-based model. Thus, a small group of 12 patients with PD (i.e., Validation Cohort) was treated with FUS unilateral subthalamotomy in the context of a pilot trial to investigate the safety and efficacy of unilateral FUS subthalamotomy in patients with PD with less than 5 years since diagnosis (*27*). Of note, the target planning was prospectively adjusted to affect more neatly onto the rostral motor STN (first lesion) to improve bradykinesia while continuing to target the posterolateral subregion aiming to improve tremor (second lesion). This modified approach resulted in a higher antiparkinsonian effect [i.e., 68.7% reduction in contralateral Movement Disorder Society–Unified Parkinson's Disease Rating Scale part III (MDS-UPDRS-III) scores]. In particular, bradykinesia was substantially more ameliorated in comparison with the Test Cohort ($n = 39$) described above (40% versus 64.2% improvement for Test and Validation Cohorts, respectively). We

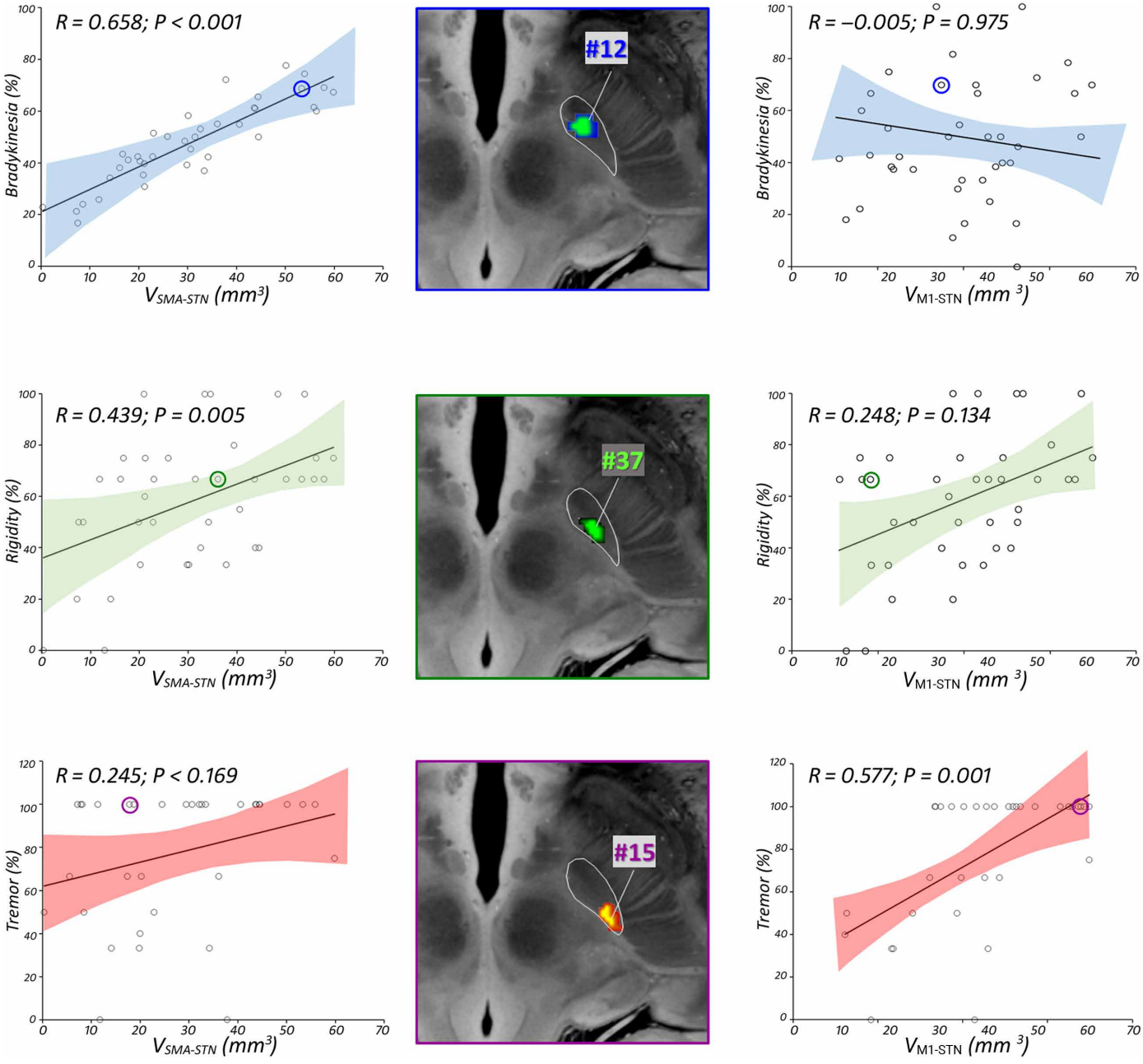

Fig. 3. Relationship between clinical outcome and lesion overlap with STN subregions. Scatterplot and 95% confidence interval (shaded area) between motor improvement and volume of the SMA-STN (**left**) and M1-STN (**right**) covered by the respective lesion. Standardized regression coefficients *R* reflect the effect of the impact on motor subregions contributing to prediction of efficacy for each motor feature (blue for bradykinesia, green for rigidity, and red for tremor). (**Middle**) Lesion reconstruction of illustrative example subjects, overlaid with an ultrahigh-resolution (100-μm) template of the human brain (*76*). Selected examples include three different patients who exhibited sign-selective response per clinical feature: bradykinesia (blue), rigidity (green), tremor (red-yellow). See table S2 for clinical details for every subject. Adjusted clinical outcomes were regressed against the other predictor variable and controlled per total lesion volume.

carried out two levels of validation analysis: local (lesion-based) and network (connectome-based) approaches.

First, overlaps of patient-specific lesions with "significant mean effect image" were used to estimate outcomes in the original data (Test Cohort, $N = 39$) in a leave-one-out manner (Fig. 5A). Estimated outcomes significantly correlated with empirical improvements for bradykinesia ($R = 0.676$; $P < 10^{-5}$), rigidity ($R = 0.585$; $P < 10^{-3}$), and tremor ($R = 0.679$; $P < 10^{-4}$). Next, we repeated the overlap calculation for the independent Validation Cohort. Predicted motor outcome was estimated based on the regression parameters from the Test Cohort. As a qualitatively assessment, "mean effect images" for this Validation Cohort are visualized in Fig. 5B, showing the spatial consistency with the original model. Namely, in this Validation Cohort, voxels with greater probability

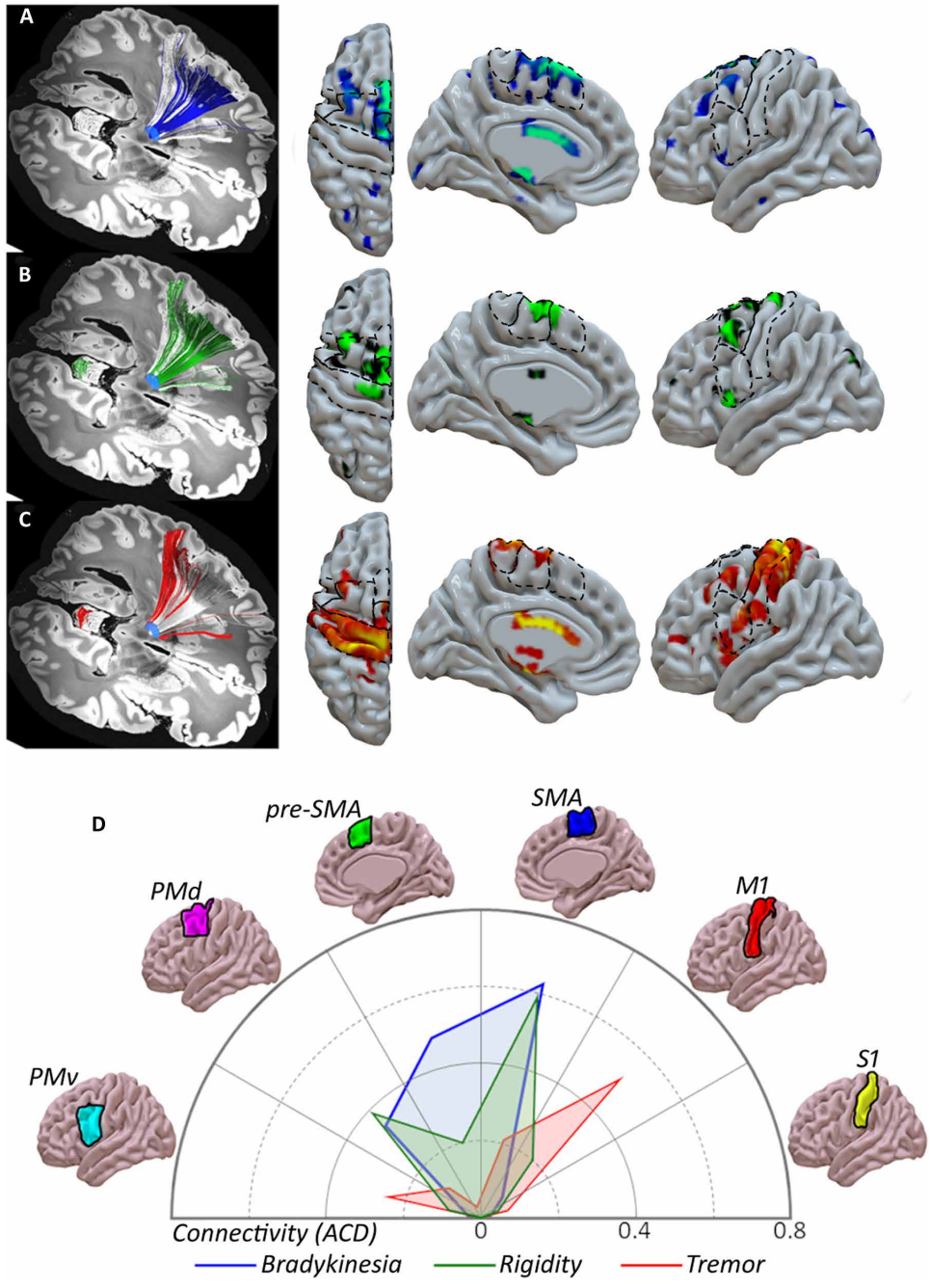

Fig. 4. Corticosubthalamic connectivity patterns of FUS-STN lesions. Sign-response tractography for bradykinesia (**A**), rigidity (**B**), and tremor (**C**). From left to right: efficacy clusters, color-coded fiber distribution from each sweet spot, and track density maps (number of tracts per vertex), overlaid on the MNI surface template (*28*). The streamline distribution seeding from lesion volumes across patients is reconstructed in white. (**D**) *ACD* values based on FUS-STN connectivity with cortical regions of interest: M1, primary motor cortex; PMd, dorsal premotor cortex; PMv, ventral premotor cortex; SMA, supplementary motor area; pre-SMA, pre-supplementary motor area; and S1, primary somatosensory cortex. Color codes are consistently related to improvement in motor features: bradykinesia (blue), rigidity (green), and tremor (red).

to improve bradykinesia and rigidity are clustered anterior-medially with respect to those with larger probability to improve tremor, which are grouped in the most posterolateral portion. In line with this spatial distribution, cross-dataset prediction revealed a significant relationship between expected and empirical improvements (Fig. 5C). Thus, the prospective adjustment in target definition according to the model built on the Test Cohort correlated with the clinical benefit found for this Validation Cohort (*27*), reinforcing its accuracy in defining the STN functional anatomy and relevance to the cardinal features of PD.

Second, as a hypothesis-driven network-based validation step, we evaluated the impact of lesion on fiber tracts associated with improvements on motor features in the Validation Cohort. Lesion connectivity profiles were obtained by isolating the fibers traversing each lesion

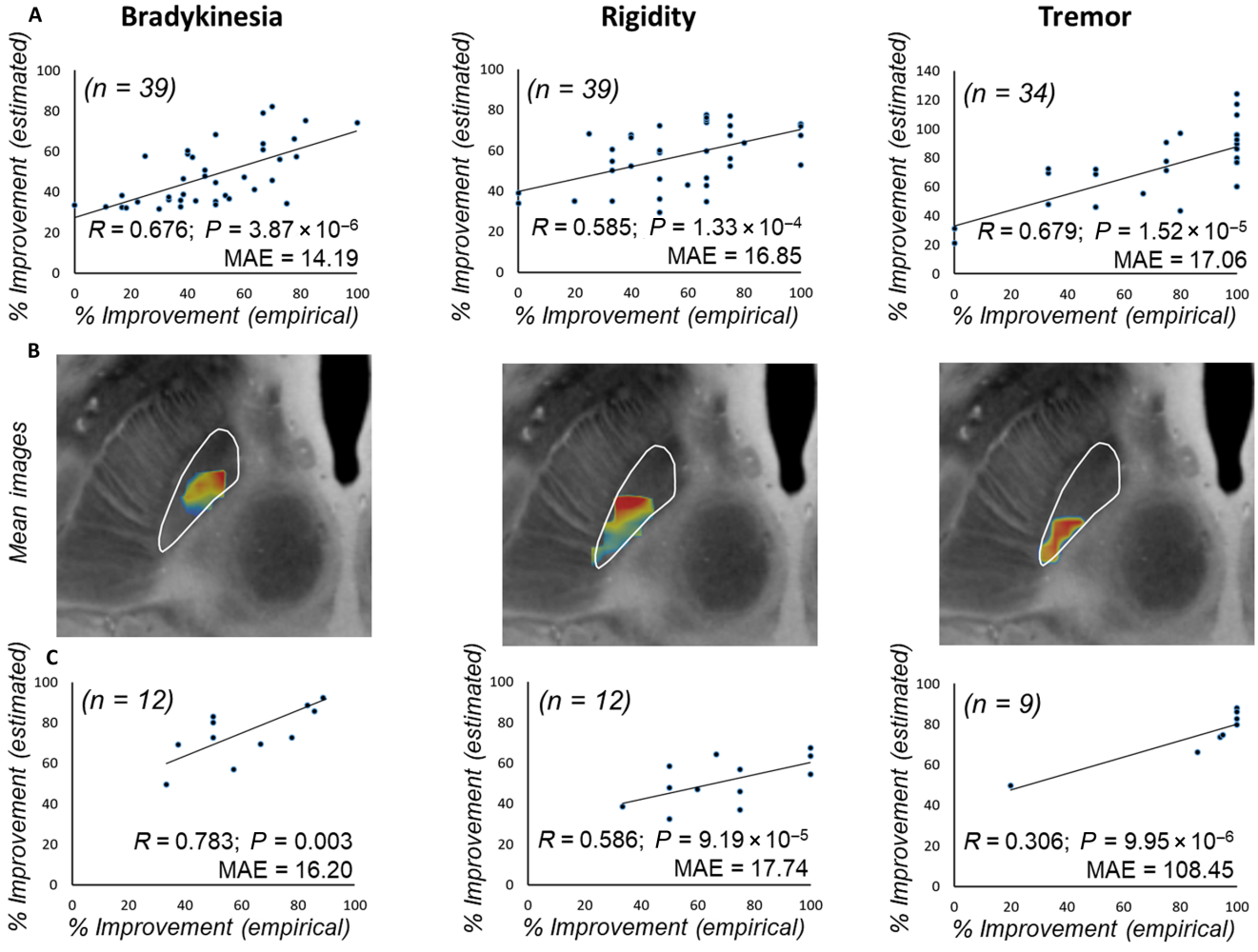

Fig. 5. Predicting FUS subthalamotomy outcome based on lesion topography. (**A**) Actual versus predicted improvement in Test Cohorts using a leave-one-out procedure. (**B**) Lesion distribution of the independent validation dataset ($n = 12$), weighted by their corresponding relative improvement for each motor sign. (**C**) Estimation of motor improvements in the Validation Cohort based on the original model from the Test Cohort, using the Spearman correlation analysis. MAE, median absolute error.

from the Human Connectome Project (HCP)-1065 dataset (*29*) and converted to tract density images in a 1-mm resolution (Fig. 6, A to C). Spatial correlations with the optimal fiber model per sign were iteratively calculated for each patient, and the resulting similarity indices were Spearman rank correlated with clinical outcomes (Fig. 6D). Tract models accounted for statistically significant amounts of variance in treatment outcome for bradykinesia (Rho = 0.817; $P = 0.0012$) and rigidity (Rho = 0.722; $P = 0.0081$). For tremor, we can observe a nonsignificant upward trend (Rho = 0.606; $P = 0.087$) for efficacy as a function of connectivity to M1. To some extent, this latter result for tremor and tractography was expected not only because of the small sample size ($n = 9$; 3 patients did not have tremor) but also because there was a marked antitremor effect (around 100%) in most cases; together, these aspects made statistical correlation elusive.

DISCUSSION

We here describe segregation of STN subregions and their cortical connectivity that are correspondingly associated with improvement in bradykinesia, rigidity, and resting tremor in PD following FUS ablation of the STN. A detailed correlation between motor behavior (i.e., improvement of clinical features) and STN anatomy has not been done previously using the impact of focal lesioning as a fundamental approach. This study has applied a methodology centered on voxel-based lesion-symptom mapping to explore the organization of the STN. Furthermore, we have elaborated on how such anatomo-clinical correlation allows interpretation of the human functional anatomy of the STN and cortical connectivity, the pathophysiology of PD, and the putative normal role of corticobasal ganglia circuits in motor control. Examining the impact of focal lesions is a traditional neuroscientific approach based on the premise that concrete neurological manifestations definitely related to specific brain lesions are directly related to the underlying (disrupted) normal function (*10*, *30*, *31*). Thus, the findings presented here are sound and reproducible. Previous assessments of STN topography and clinical efficacy have been directed by and large to defining the most effective placement for DBS electrode location (*14*–*17*). However, a recent study by Rajamani *et al.* (*18*) reported a similar topographic organization for STN-cortical connectivity based on the effect of DBS electrodes. This will be discussed in more detail below.

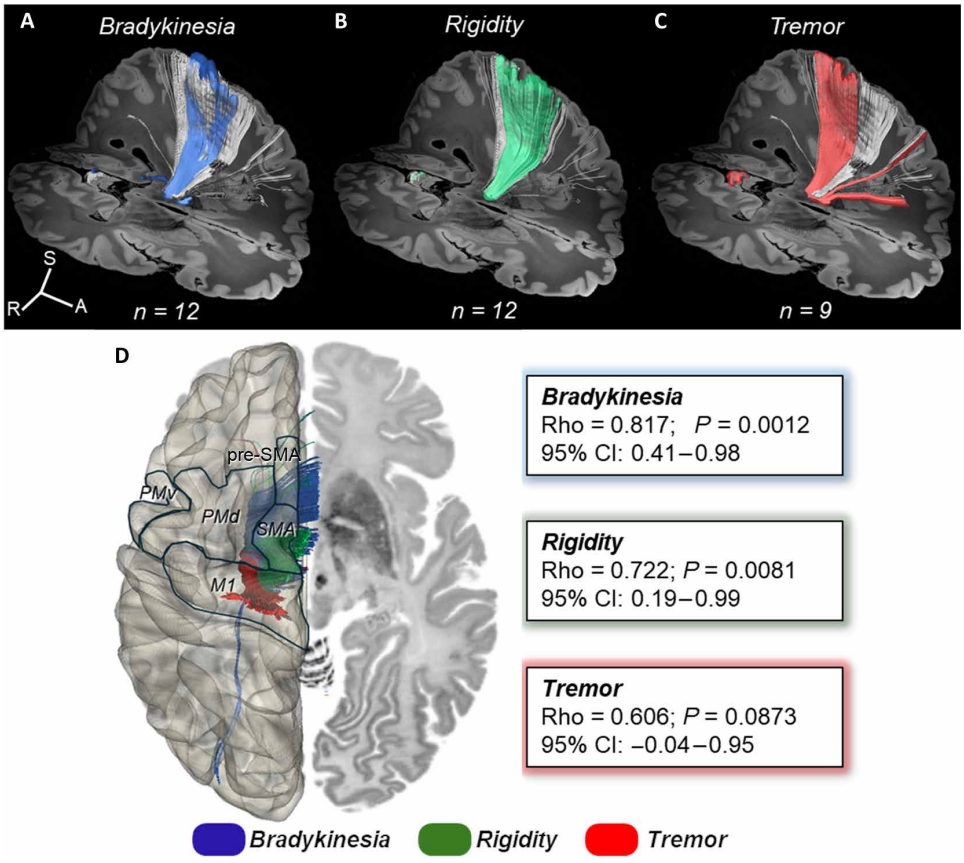

Fig. 6. Predictive fiber tracts in Validation Cohort. (Top) All fibers connected to the sum of lesions in the Validation Cohort are shown in white. Predictive fibers associated with improvement in bradykinesia (**A**), rigidity (**B**), and tremor (**C**) are color coded. (**D**) (Left) Cortical projections of color-coded streamlines associated with motor improvements. Motor cortical regions from a human motor area template (*28*) are delineated in a semitransparent brain surface in the MNI space. (Right) Streamlines were transformed to tract density images, and degrees of effective fibers affected by single lesions were rank correlated in a voxel-wise manner with motor improvement across the Validation Cohort. *P* values are based on Spearman correlations with bootstrapping resampling (1000 replications). See fig. S5 for associated tract density images. Rho, Spearman *R*; 95% CI, 95% confidence interval.

STN-cortical connectivity and motor improvement

The impact on the cardinal features of PD encountered in this study is highly specific and relevant in terms of motor outcome and lesion topography. In our two initial studies (i.e., pilot and double-blind controlled studies), we found that FUS-STN improved tremor the most (77 and 83%) and bradykinesia the least (37 and 33%), with intermediate benefit for rigidity (71 and 60%) (*25*, *26*). A lesser effect on bradykinesia had also been encountered with STN-DBS (*18*), but the anatomo-functional basis for such differential effects was not explained at the time (*32*).

The variability in the clinical response seen in our patients allowed correlation with topography, which reveals a net anterior-posterior and mediolateral gradient within the STN predicting the degree of improvement of each cardinal feature. This, in turn, coincides quite precisely with the intranuclear STN representation of the SMA and M1, which are anterior-medially and posterior-laterally placed in the STN and their corresponding cortical connectivity, respectively (*3*, *5*–*7*). In addition, we have established a statistically robust relationship between anteriorly placed lesions impinging on the SMA-STN subregion and improvement in bradykinesia, whereas caudally and laterally placed lesions affecting the M1-STN convey the greatest antitremor effect (Fig. 2A). This was corroborated by the multiple regression analysis. Furthermore, the cortical connectivity approach confirmed that the relationship between affecting the SMA-STN and bradykinesia improvement and impingement on M1-STN connectivity induced the greatest benefit against parkinsonian resting tremor. The optimal topography of ablation associated with amelioration of rigidity overlapped mostly with connectivity of the anterior motor STN and cortical premotor areas (Figs. 2B and 4). Of note, our connectivity analysis revealed some other interesting associations (Fig. 4). Thus, the STN antitremor site showed the strongest connectivity not only with M1 but also with PMv, whereas improvement in bradykinesia localized to the rostral STN motor region connected to not only SMA but also pre-SMA and PMd. The findings for rigidity are somewhat less notably defined but highly interesting. Thus, STN-cortical connectivity for rigidity mostly coincided with the one for bradykinesia but is more limited to SMA and PMd (Fig. 4).

This clinical topography coincides by and large with a recent study by Rajamani *et al.* (*18*) in a large cohort ($N = 237$) of patients with PD operated for bilateral DBS in five centers. In this highly elaborate study, a significant association between the stimulation of tracts connecting the posterior STN with the M1 and cerebellum (secondary analysis) and tremor improvement was found, whereas

connectivity between the anterior motor and premotor STN with the SMA and pre-SMA was associated with improvement in bradykinesia and rigidity (*18*). The results were further validated in another cohort ($N = 93$ patients) from three independent centers. Accordingly, the results of Rajamani *et al.* (*18*) also established a fairly firm topography between motor improvement of tremor and best efficacy at the level of the posterior STN-M1 connection and more rostral STN-cortical premotor areas connectivity for akinesia-rigidity.

Our findings using focal ablation as the main methodology fit quite well with those encountered with DBS, together providing a strong indication of a segregated pattern of corticosubthalamic connectivity and motor manifestations. Accordingly, a rostrocaudal STN-cortical organization probably underlies relatively distinct mechanisms involved in bradykinesia, rigidity, and tremor in PD, which, in turn, could be used to make some broad deductions regarding basal ganglia mechanisms in normal motor control and behavior (Fig. 7). This is in keeping with the recent detailed study by Hollunder *et al.* (*33*), which describes a rostrocaudal cortico-STN connectivity organization associated with benefit by STN-DBS in several motor disorders (i.e., dystonia and PD) and behavioral disorders (Tourette's syndrome and obsessive-compulsive disorder). Accordingly, primary motor manifestations and their improvement are mediated by more caudal corticobasal ganglia connectivity and the opposite, behavioral disorders are more rostrally mediated in the brain (*33*, *34*). Admittedly, there is a relevant degree of functional and anatomical overlap within the organization of the STN as much as for other basal ganglia nuclei (*35*, *36*). Nevertheless, we believe the data we report here are robust and have been supported by different analytic approaches, which, in addition to a wealth of experimental and clinical findings, strongly support the existence of segregated STN-cortical connections and cardinal features of PD. Of note, the main hypothesis was retested prospectively by adapting our lesioning approach for FUS subthalamotomy in an out-of-sample cohort (Validation Cohort) of patients with PD (*27*). Thus, the planning of lesion targeting was modified to enlarge the impact on the rostral motor STN subregion with the aim of affecting the STN area projecting to premotor cortices and therefore better improvement in bradykinesia. This strategy proved to be correct, and this latter hypothesis-driven analysis showed that it was the volume of ablation in the rostral motor STN (i.e., connected to SMA and premotor cortices) that predicted the outcome on bradykinesia and

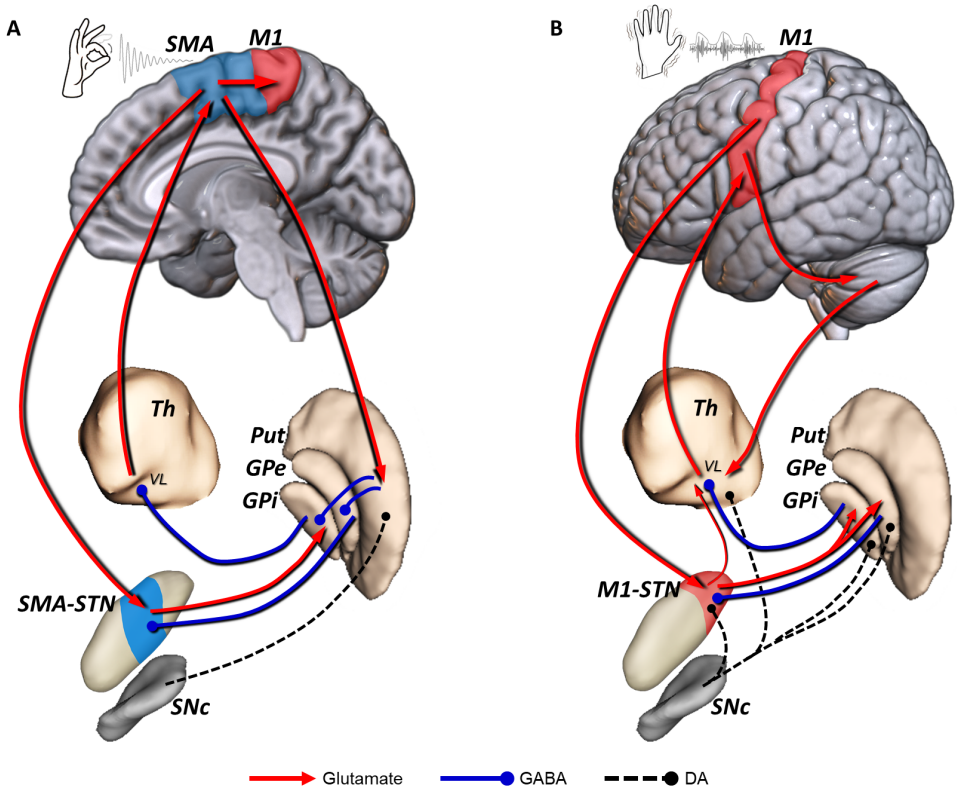

Fig. 7. Segregated circuits for bradykinesia and resting tremor in PD. (**A**) Loss of nigrostriatal DA changes the regulation of direct/indirect pathways and leads to an abnormal firing pattern in the rostral motor STN (SMA-STN), which is connected with the motor cortex through the SMA-STN hyperdirect pathway. This altered neuronal activity is also present in the rostral area of the motor GPi, which, in turn, projects to the VL thalamus and leads to excessive inhibition of the thalamo-cortical excitatory projection to the motor cortex, particularly SMA. (**B**) Dopaminergic extrastriatal loss modifies the balance of the STN-GPe microcircuitry (i.e., excitation/inhibition), giving rise to abnormal oscillatory activity at 4 to 6 Hz. This resting tremor activity is found within the most caudal area of the motor STN (M1-STN). Tremor activity probably reaches the cortex through the thalamo-cortical projection to the M1. The cerebello-thalamo-cortical network contributes to the maintenance and amplification of resting tremor triggered by peripheral feedback, and possibly the M1-STN hyperdirect pathway reinforces the oscillatory activity within the STN. A putative direct subthalamo-thalamic connection (*77*), which might facilitate tremor propagation from the STN-GPe pacemaker to the motor cortex through the thalamus, has not been described in humans. DA, dopaminergic; GPe, globus pallidus pars externa; GPi, globus pallidus pars interna; M1, primary motor cortex; Put, putamen; SNc, substantia nigra pars compacta; STN, subthalamic nucleus; Th, thalamus; SMA, supplementary motor area; VL, ventrolateral thalamus; GABA, γ-aminobutyric acid.

rigidity (64.2 and 69.6% amelioration, respectively). In keeping with the high predictive value of the model, the posterolateral impact on the STN subregion/M1 connection accounted for a high tremor effect (90.3% improvement). Together, these findings fit well with an STN-cortical segregated pattern with a rostrocaudal gradient for bradykinesia, rigidity, and tremor in PD.

Pathophysiology of cardinal features of PD

Extensive previous evidence has shown that bradykinesia in PD is mainly related to dysfunction of the premotor cortical areas (*37*–*41*). Our results indicate meaningful connectivity of clinically effective STN lesions for bradykinesia with the supplementary motor complex and PMd (i.e., area 6). The former has been preferentially associated with planning of self-induced movements and actions, whereas the latter appears to play a role in anticipating and executing externally cued movements (*42*). Animal experiments using anterograde axonal tracing have demonstrated that the premotor cortex (PMC) projects to the medial aspect of the STN but largely overlaps the SMA region (*35*, *36*). On the contrary, PMC and SMA projections to the M1 and striatum are topographically segregated (*43*). These results are consistent with the involvement of pre-SMA, SMA, and PMd in different aspects of bradykinesia (*44*) and the vast and diverse aspects of human motor repertoire (*33*, *45*).

Improvement in rigidity in our study showed a fairly high match with the connectivity pattern of bradykinesia, excepting the pre-SMA. It is tempting to suggest that rigidity and its associated enhancement of the stretch reflex in PD (*46*) could be primarily associated with the PMd connection (*5*, *35*, *36*) and the hyperdirect cortico-STN projection (*47*). This fits with the proximal joint fixation and posturing function attributed to PMd. Our results coincide by and large with previous (*15*) and more recent definitive results of rostral STN-cortical connectivity best associated with improvement of bradykinesia and rigidity (*18*). Admittedly, there are some few differences between results derived from ablation and DBS, which, after all, are not too unexpected, considering not only the distinct mechanism of action of either method but also the different spatial orientation and spreading of DBS electric fields and FUS-delivered thermal dose.

Tremor is arguably the most specific sign of PD; however, a sound explanation of its origin in PD has evaded historical and modern attempts. Of note, there is no correlation between striatal dopamine depletion and tremor in PD (*48*), which is also generally less responsive to dopaminergic medication. How dopaminergic loss leads to 4- to 6-Hz neuronal synchronous firing is not yet clear. Our results neatly show that tremor is associated not only with the posterior-lateral motor STN and its connection with the M1 but also with the PMC-ventral area and, to a lesser extent, with the SMA. The exquisite focal and distal presentation of resting tremor in most patients suggests a somatotopic cortical mechanism, which could well be mediated by the M1/STN and PMv-STN hyperdirect projections (*49*). PMv neurons are highly responsive to peripheral somatosensory afferents and become preferentially activated with distal hand actions (*50*). Peripheral feedback sustains and may even enhance tremor via the cerebello-thalamo-cortical network (*20*). Cerebellar cortical output goes mainly not only to M1 but also to PMC and SMA projections (*51*, *52*), which may also be part of the oscillatory network. Our study did not ascertain STN-cerebellar connectivity specifically; however, cerebellar engagement in PD tremor is indisputable (*20*, *53*) and is also in keeping with the findings of Rajamani *et al.* (*18*). It is noteworthy, however, that the cerebellum does not receive dopaminergic innervation or direct monosynaptic connections from the basal ganglia as far as is known today (*54*). On the other hand, the well-established disynaptic connectivity between the STN and dentate nucleus (via the pons) (*55*) could certainly play a relevant role in engaging the cerebellar network to sustain (or enhance) tremor (the "dimmer-switch" model) (*19*, *55*, *56*). The possibility that our therapeutic ablations could impinge on the dentato-rubro-thalamic (DRT) projection should be considered given previous results with DBS (*57*), but examining the impact of lesions on the white matter structures surrounding the STN is beyond the scope of this research. Moreover, lesioning the DRT seems unlikely because we found tremor benefit related to posterolateral lesions. They are relatively distant from the course of the DRT, and there was no correlation between the total volume of the lesion and tremor improvement. We suggest a prominent role of extrastriatal dopaminergic innervation, particularly putative changes in the reciprocal STN–globus pallidus pars externa (GPe)–globus pallidus pars interna (GPi) microcircuitry (*58*, *59*), giving rise to the abnormal oscillatory activity of tremor in PD (Fig. 7B) (*60*). However, how such abnormal oscillatory 4- to 6-Hz activity accesses the M1-corticospinal projection to reach the spinal cord and muscle segments in a somatotopic organized manner is not clear.

Last, our finding supports historical and modern notions that bradykinesia and rigidity are principal manifestations of basal ganglia dysfunction and most likely represent the clinical counterpart of a fundamental role of the basal ganglia in motor control (i.e., movement selection and energization) (*8*, *61*, *62*) mediated by corticostriatal and striatopallidal direct and indirect projections principally toward cortical premotor areas. On the other hand, the physiological counterpart of the 4- to 6-Hz oscillatory activity of rest tremor remains unexplained. The fact that tremor at rest is exclusively present in humans is more prominent in distal joints of the limbs and the typical repetitive 4- to 6-Hz movements exhibit well-organized reciprocal inhibition suggest together that tremor uses motor cortical mechanisms developed for refined and well-learned hand and finger movements, such as picking up and selecting objects, self-purging, etc., which tend to be repetitive and rhythmic. Accordingly, we suggest a dual corticobasal ganglia organization that sustains different aspects of movement control, i.e., selection and acquisition of motor programs versus performance of highly automatized actions (Fig. 7).

Methodological issues and limitations

First, this study consisted of a retrospective topographic analysis of a relatively small cohort (39 patients) who underwent subthalamotomy in two prospective clinical studies of FUS-STN for PD (*25*, *26*). Our approach was rather standardized in an effort to improve all cardinal motor features in patients with asymmetric PD stemming from previous experience with radiofrequency-mediated subthalamotomy (*63*, *64*). No systematic mapping of the STN was attempted purposely to explore the variable clinical response associated with different sites within the nucleus, which explains the high degree of lesion overlap. As a consequence, an intrinsic limitation of this approach is the autocorrelation of the data, increasing the likelihood of false positives. Moreover, voxel-based lesion-symptom mapping implements a massive univariate regression model to relate clinical outcome to the spatial distribution of lesions, thus leading to the issue of multiple comparisons. In this study, we used a nonparametric

rank order test (*65*) that has been shown to be less sensitive to false positives than parametric permutations (*66*). Following a previous proposal (*67*), only voxels that survived correction for multiple comparisons were validated as belonging to the significant mean effect image for each motor feature. Any voxels that did not reside within the atlas-defined STN and those that received clinical scores from less than 10 lesions were discarded. This anatomically informed approach conforms to the study hypothesis, ensures the validity of voxel-wise statistical tests, and accounts for the risk of the "regression to the mean" error. Admittedly, functionally relevant areas might have been missed because they are beyond the analyzed regions or did not exceed the predefined thresholds.

Second, manual segmentation of the lesions and limited MRI resolution could introduce some variability. A proportion of the estimated acute FUS lesion as evaluated by MRI (24 hours after the procedure) probably did not evolve into tissue necrosis, thus leading to overestimation of lesion volume. The latter is more likely as the distance from the sonicated target increases, where it is more probable that the tissue experienced heating-evoked edema rather than necrosis. Nonetheless, the core of the lesion encountered mainly within the STN (V_{STN}) should be mostly necrotic (*68*). Another potential pitfall is that nonlinear warping of lesions into the standard MNI space may become a source of bias. However, localization in the standard MNI space of both lesions and DBS (i.e., electrodes and volume of tissue activated) has been successfully and extensively used to explain clinical outcomes in previous studies (*14*, *64*). The nonlinear registration method used in this study has been shown to account for intersubject anatomical variability more effectively compared with other nonlinear deformation algorithms (*69*). This diffeomorphic approach preserves local anatomical details while generating smooth transformations, thereby reducing spatial distortions and ensuring optimal alignment of relevant structures. The creation of study-specific templates tailored to the population under investigation enhances the sensitivity and specificity of lesion localization analyses. In addition, registration processes were rigorously monitored by visual inspection, and patient-specific adjustments were made when necessary.

Connectivity analyses were assessed on a population-averaged connectome based on diffusion data from 1065 participants of the HCP (*29*). It is expected that the use of normative data introduces limitations regarding the anatomical accuracy and the ability to capture patient-specific variability in brain pathways. However, the use of individualized structural connectivity has practical limitations, such as small sample size, suboptimal resolution, and poorer signal-to-noise ratio. Besides, the presence of movement artifacts is especially relevant in a sample cohort of patients with PD. The advantage of normative connectomes lies in the use of advanced acquisition and processing tools, resulting in higher image quality than could be achieved during clinical routine. Previous studies in DBS have confirmed that the use of normative models resulted in highly similar connectivity profiles in comparison with patient-specific diffusion data, leading to similar conclusions about the sweet spots associated with optimal clinical improvement (*18*, *33*, *70*). Nevertheless, although our data significantly accounted for variation in clinical outcome in both the Test and Validation Cohorts, its usefulness in FUS-STN targeting should be prospectively validated in patient-specific data.

The clinical-topographic model of the STN was prospectively tested in 12 patients with PD. Patients in this cohort presented less than 5 years from diagnosis (early PD), which implies a substantial difference from the Test Cohort. Such heterogeneity could decrease our power for predicting the clinical outcome based on the lesion model. However, that our predictions were significant despite this heterogeneity could be seen as a strength, and one would expect improved reproducibility in other cohorts.

In addition, two other methodological and conceptual aspects are worth considering. The functional (i.e., clinical) impact of a focal brain lesion is not limited or solely mediated by tissue elimination in a given region but carries a network effect. However, the impact of focal ablation is principally mediated by interrupting afferent/efferent activity from the lesioned nucleus, thus having a local blocking effect. This is unlike the effect of DBS, which involves several local and distant physiological mechanisms, including modulation of surrounding tracts (*21*). Moreover, our findings were confirmed regarding the patient-based relationship between the distributed topography of the FUS-STN lesions and the organization of the STN according to a connectivity-based atlas (Fig. 3) (*7*) by the complementary population-based corticosubthalamic connectivity analysis (Fig. 4). In the latter approach, the connection strength between two regions (i.e., each STN subregion and the corresponding cortical area) was considered proportional to the total area comprised by the fiber connector volume over the surfaces of the two related structures. Therefore, the number of streamlines isolated by each sweet spot acquired a biological significance related to the clinically effective interruption of information flow between the connected areas (for example, the SMA-STN projection and improvement in bradykinesia). Furthermore, these results were replicated in the Validation Cohort.

Our results tested by several methodological approaches allow us to establish a near to causal relationship between the topography of the ablation, the specific improvement of each motor sign, and the STN-cortical projection areas. Thus, most favorable outcomes for bradykinesia and rigidity were associated with lesioning the rostral STN motor subregion connected to premotor cortical areas, whereas tremor improved the most with posterior-lateral STN lesions connected to the M1 and ventral PMC. These results may also serve to tailor STN interventions for PD to each patient's individual clinical presentation, optimizing clinical outcomes and the risk-to-benefit ratio of functional procedures.

MATERIALS AND METHODS

Patients

Between April 2016 and May 2019, a total of 45 patients with asymmetric PD underwent unilateral FUS-STN in an initial pilot study (*25*) or a subsequent randomized sham-controlled double-blind trial, respectively (*26*). Four patients were lost to follow-up due to COVID-19 pandemic restrictions, and two patients who developed limb weakness allegedly caused by partial extension of ablation to the internal capsule were excluded due to residual clumsiness interfering with bradykinesia assessments (fig. S1) (*26*). Thus, 39 patients were included in this Test Cohort for a retrospective topographic analysis of FUS-STN lesions (table S1). A lesion-based model was prospectively tested in a Validation Cohort consisted of 12 patients, included in a pilot trial to investigate the safety and efficacy of unilateral FUS subthalamotomy (*27*). All the studies were performed according to the Helsinki Declaration and approved by the local Ethics Committee, and all patients provided written informed

consent. These studies were registered with ClinicalTrials.gov with numbers NCT02912871, NCT03454425, and NCT04692116, respectively.

Clinical assessments

The MDS-UPDRS-III (*71*) was assessed in both "off" (≥12 hours after withdrawal of dopaminergic medication) and "on" (60 to 120 min after their habitual dose of levodopa) states. For the analyses undertaken in this study, only off-medication evaluations were considered as they provide the net effect resulting from subthalamotomy. Motor scores for bradykinesia, rigidity, and tremor were calculated as the sum of MDS-UPDRS-III subscores from the most affected (i.e., treated) side. Contralateral score for rigidity ranges from 0 to 8 (item 3.3), contralateral score for bradykinesia ranges from 0 to 20 (items 3.4 to 3.8), and contralateral score for resting tremor ranges from 0 to 8 (items 3.17). In all cases, unilateral assessment includes evaluation in the upper and lower limbs, with higher scores indicating worst motor performance. Assessments were conducted at baseline, 4-month (± 4 weeks), and 12-month (± 8 weeks) follow-up.

FUS subthalamotomy procedure

FUS-STN was performed in an ExAblate 4000 system (Insightec, Haifa, Israel), which consists of an MR-compatible 1024-element ultrasound transducer array. Ultrasound beams penetrate through the intact skull and focus on a targeted deep brain structure to create a thermal ablation. The brain tissue temperature is increased progressively, and the procedure is monitored in real time by clinical examination and MRI, including thermography. Our group strategy for FUS-STN generally included sonicating of three targets within the motor STN. Once the anterior commissure–posterior commissure line was marked, the first target was located 12 mm lateral to midline, 3 mm caudal, and 3 mm ventral to the mid-commissural point. Registered pre- and intratreatment MRI was used to adjust the target according to the patient's anatomy. After achieving at least three effective (≥54°C) sonications along with clinical improvement, the ultrasound focus was moved ≈1 mm caudal and ≈1 mm lateral and the procedure was repeated while looking for greater clinical improvement, particularly an antitremor effect. Last, the target was moved 1 mm dorsally and ≈0.5 mm medially and rostrally with respect to the initial target to enlarge the lesion dorsal-medially onto the fields of Forel, aiming to affect the pallidothalamic fibers (*64*). The procedure was ultimately guided by the clinical response. In particular, side effects such as motor weakness, dysarthria, and dysmetria were checked regularly after each sonication, and target coordinates were corrected as needed.

Image acquisition and segmentation

Baseline T1w (3D-MPRAGE, voxel size = 1.0 mm^3) and 24-hour posttreatment T1w and T2w (FSE, voxel size = 0.5 by 0.5 by 2.0 mm^3) images were acquired on a 3-T MRI (General Electric, Milwaukee, United States). T1w and T2w sequences were rigidly transformed to the baseline T1w images. A nonlinear spatial registration algorithm [DARTEL (Diffeomorphic Anatomical Registration Through Exponentiated Lie Algebra), as implemented in SPM12 (http://fil.ion.ucl.ac.uk/spm/software/spm12/) (*72*), was applied to baseline T1w volumes to estimate a nonlinear deformation field into the MNI152-NLIN2009 asymmetric space. A connectivity-based atlas, which features a quadripartite STN model 6, was resliced and registered to individual native spaces by applying the inverse of the subject-specific warp field. Each transformation was visually validated and, if necessary, refined using an additional affine transformation step in the 3D Slicer software (https://slicer.org/).

Acute FUS lesion boundaries were manually segmented in the native space using the ITK-Snap software (http://itksnap.org). To characterize the lesion, two zones (i.e., necrotic core and periphery) were simultaneously segmented on registered T1w and T2w volumes representing zones 1 and 2 for FUS ablative procedures according to Wintermark *et al.* (*68*). Lesion voxels in zone 1 were hyperintense in T1w and hypointense in T2w, whereas lesion voxels in zone 2 were hypointense in T1w and hyperintense in T2w. All images were segmented by two of the authors (R.R.-R. and J.U.M.-M.), and only voxels that were labeled as lesions by both raters were included in the final segmentation. To determine the extent of interrater variability, the kappa similarity coefficient was calculated for all labels following segmentation.

Topography analysis

Registered atlases were used to create individualized masks of the STN and the regions corresponding to M1, SMA, associative, and limbic connections (*7*). Total lesion volume (V_{TOT}) was calculated as the sum of zones 1 and 2. The effective lesions in the STN (V_{STN}) were calculated by computing the voxels that are common to the lesion and the STN and saved for subsequent voxel-based analysis. Overlap of patient-specific lesions with the M1 ($V_{M1\text{-}STN}$), SMA ($V_{SMA\text{-}STN}$), associative ($V_{ASSOC\text{-}STN}$), and limbic ($V_{LIMBIC\text{-}STN}$) subregions of the STN was computed based on the correspondent masks defined by the quadripartite STN atlas (*7*). Subsequently, each lesion was transformed to the MNI152-NLIN2009 space using the corresponding transformation matrix.

Spatial relations between STN functional topography and FUS-STN efficacy

Mapping voxel-based lesion-symptom mapping

Our probabilistic mapping strategy follows, in general, previously proposed approaches (*67*, *73*). Patient-specific lesions were first weighted by their corresponding relative improvement from baseline as assessed by the MDS-UPDRS-III scale. Mean effect images were computed for each score in a voxel-wise manner by averaging the sum of all weighted volumes overlapping a given voxel. In parallel, an unweighted "n-map" was generated, which included the total number of volumes overlapping each voxel. To ensure the validity of voxel-wise statistical testing, the n-map was thresholded to contain voxels occupied with at least 10 lesions (*67*) and then used to mask the mean effect images.

The association between lesion status and clinical improvement was tested for each remaining voxel. Because of the non-normal distribution of our data, voxel-wise, nonparametric Brunner-Munzel rank order tests were performed, as implemented in the NPM software (https://nitrc.org/projects/mricron) (*65*, *66*). As proposed by Medina *et al.* (*74*), we used a permutation-derived correction to address the type I error that is inherent in voxel-wise statistical analysis. Voxels with values exceeding a false discovery rate (FDR) of $P < 0.05$ were considered significant and stored in a "*P*-map." Last, the n-masked mean effect images were thresholded by using the corrected *P*-maps to create a significant mean effect image for each clinical feature. Subsequently, these maps were binarized and rendered, and respective centers of mass were computed in the MNI152-NLIN2009 space.

Subthalamic signotopy

Hypothesis-driven hierarchical multiple regression analyses were used to examine the relationship of lesion topography to clinical outcome. For each motor outcome, the efficacy, measured as % of change, was modeled as a linear combination of the volume of lesion impacting in each functional parcel ($V_{CX\text{-}STN}$) as independent variables. The total volume was primarily entered as a nuisance variable in the regression model and regressed out to control for larger, less focal lesions. A value of $P < 0.05$ was considered to indicate statistical significance.

Connectivity

To scrutinize the relationship between the impact of effective lesions on corticosubthalamic pathways and clinical outcome, we developed a structural connectivity analysis defined by a high-resolution, population-averaged atlas in the MNI space (ICBM 2009a Nonlinear Asymmetric template), available in the HCP-1065 dataset (*29*). This probabilistic tractography atlas is shared with the DSI-Studio package and is publicly available at http://dsi-studio.labsolver.org. To assess the topography of feature-related connections, we seeded streamlines from each binarized significant mean effect image separately. The end/terminate regions were set on six regions defined by a human motor area template: M1, PMd, PMv, SMA proper, pre-SMA, and primary somatosensory cortex (S1) (*28*). A total of 50,000 seeds by region was explored, and a maximum of 500-mm trace length and a curvature threshold of ±90° were imposed as tracking parameters. The individual seed-region connectivity was computed through the anatomical connection density (*ACD*) matrices (*75*). *ACD* values, ranging from 0 to 1, reflect the fraction of the region's surface involved in the axonal connection with respect to the total surface of both regions (see the Supplementary Materials).

Last, track density imaging (TDI) maps with 1-mm isotropic voxels were generated from each isolated track, masked with cortical regions of interest, and projected onto an inflated brain surface in the MNI space using the Surf Ice software (https://www.nitrc.org/projects/surfice). This enabled us to delineate the cortical topography of sign-related mappings as vertex intensity in TDI reflects the density of streamlines within the voxel.

Cross-validation and testing

To test the reproducibility and consistency of the findings and the value of STN functional anatomy parcellation described here for clinical decision-making, we first performed a retrospective validation analysis, simulating motor scores in the Test Cohort based solely on the overlap of lesion volumes with the correspondent significant mean effect image (i.e., bradykinesia, rigidity, and tremor). To account for the circular nature of this analysis, the ability of the sweet spot and connectivity models to predict motor improvements was prospectively tested on an additional FUS-STN Validation Cohort ($N = 12$). Those patients were included in a pilot trial to investigate the safety and efficacy of unilateral FUS subthalamotomy in "early" (<5 years of evolution) patients with PD. The clinical results have been reported elsewhere in detail (*27*). Imaging acquisition, segmentation, and normalization of the lesions to the MNI space were undertaken with the same methodology as described above.

Validation analysis was carried out at two levels. In the first, local analysis, the voxel-based overlap of individual lesions with each significant mean effect image was used to explain clinical improvement within the Test Cohort through a linear regression model. To evaluate the strength of the model, we correlated predicted and empirical individual motor score improvements in a leave-one-out design. The median absolute error was computed to quantify the discrepancy with the measured improvement, and permutation-based testing was conducted to correct for a type I error. To further test robustness, we used the regression parameters calculated in the Test Cohort" to cross-validate the model within the Validation Cohort.

The second, connectome-based analysis was carried out using data from the ($N = 12$) Validation Cohort. Patient-specific streamlines were isolated from the high-resolution HCP-1065 connectome through association with individual lesions and converted to TDI maps (voxel resolution = 1-mm isotropic). Track fibers were modeled with the same pipeline as the patient's Test Cohort. Each patient-derived TDI map was then tested in a voxel-by-voxel basis for spatial similarity with the optimal connectivity TDI derived from the sweet spots (Supplementary Materials). The resulting similarity index was Spearman rank correlated with clinical outcomes for each motor feature. Rank correlation coefficients were thresholded at a P value of <0.05 after Bonferroni correction.

Supplementary Materials

The PDF file includes:

Figs. S1 to S5
Tables S1 and S2
Legends for data S1 and S2
References

Other Supplementary Material for this manuscript includes the following:

Data S1 and S2

REFERENCES AND NOTES

1. M. R. DeLong, T. Wichmann, Basal ganglia circuits as targets for neuromodulation in Parkinson disease. *JAMA Neurol.* **72**, 1354–1360 (2015).
2. P. Krack, J. Volkmann, G. Tinkhauser, G. Deuschl, Deep brain stimulation in movement disorders: From experimental surgery to evidence-based therapy. *Mov. Disord.* **34**, 1795–1810 (2019).
3. W. I. Haynes, S. N. Haber, The organization of prefrontal-subthalamic inputs in primates provides an anatomical substrate for both functional specificity and integration: Implications for Basal Ganglia models and deep brain stimulation. *J. Neurosci.* **33**, 4804–4814 (2013).
4. M. C. Keuken, H. B. M. Uylings, S. Geyer, A. Schäfer, R. Turner, B. U. Forstmann, Are there three subdivisions in the primate subthalamic nucleus? *Front Neuroanat.* **6**, 14 (2012).
5. A. Nambu, M. Takada, M. Inase, H. Tokuno, Dual somatotopical representations in the primate subthalamic nucleus: Evidence for ordered but reversed body-map transformations from the primary motor cortex and the supplementary motor area. *J. Neurosci.* **16**, 2671–2683 (1996).
6. H. Iwamuro, Y. Tachibana, Y. Ugawa, N. Saito, A. Nambu, Information processing from the motor cortices to the subthalamic nucleus and globus pallidus and their somatotopic organizations revealed electrophysiologically in monkeys. *Eur. J. Neurosci.* **46**, 2684–2701 (2017).
7. R. Rodriguez-Rojas, J. A. Pineda-Pardo, J. Manez-Miro, A. Sanchez-Turel, R. Martinez-Fernandez, M. Del Alamo, M. DeLong, J. A. Obeso, Functional topography of the human subthalamic nucleus: Relevance for subthalamotomy in Parkinson's disease. *Mov. Disord.* **37**, 279–290 (2022).
8. C. D. Marsden, The mysterious motor function of the basal ganglia: The Robert Wartenberg Lecture. *Neurology* **32**, 514–539 (1982).
9. P. Redgrave, M. Rodriguez, Y. Smith, M. C. Rodriguez-Oroz, S. Lehericy, H. Bergman, Y. Agid, M. R. DeLong, J. A. Obeso, Goal-directed and habitual control in the basal ganglia: Implications for Parkinson's disease. *Nat. Rev. Neurosci.* **11**, 760–772 (2010).
10. J. A. Obeso, M. Jahanshahi, L. Alvarez, R. Macias, I. Pedroso, L. Wilkinson, N. Pavon, B. Day, S. Pinto, M. C. Rodríguez-Oroz, J. Tejeiro, J. Artieda, P. Talelli, O. Swayne, R. Rodríguez, K. Bhatia, M. Rodriguez-Diaz, G. Lopez, J. Guridi, J. C. Rothwell, What can man do without basal ganglia motor output? The effect of combined unilateral subthalamotomy and pallidotomy in a patient with Parkinson's disease. *Exp. Neurol.* **220**, 283–292 (2009).
11. H. Narabayashi, T. Okuma, S. Shikiba, Procaine oil blocking of the globus pallidus. *AMA Arch Neurol. Psychiatry* **75**, 36–48 (1956).

12. R. Hassler, T. Riechert, F. Mundinger, W. Umbach, J. A. Ganglberger, Physiological observations in stereotaxic operations in extrapyramidal motor disturbances. *Brain* **83**, 337–350 (1960).
13. H. Narabayashi, "Muscle tone conducting system and tremor concerned structures" in *Third Symposium on Parkinson's Disease*, F. J. Gillingham, I. M. L. Donaldson, Eds. (Livingstone, 1969), pp. 246–251.
14. A. Horn, W. J. Neumann, K. Degen, G. H. Schneider, A. A. Kühn, Toward an electrophysiological "sweet spot" for deep brain stimulation in the subthalamic nucleus. *Hum. Brain Mapp.* **38**, 3377–3390 (2017).
15. H. Akram, S. N. Sotiropoulos, S. Jbabdi, D. Georgiev, P. Mahlknecht, J. Hyam, T. Foltynie, P. Limousin, E. De Vita, M. Jahanshahi, M. Hariz, J. Ashburner, T. Behrens, L. Zrinzo, Subthalamic deep brain stimulation sweet spots and hyperdirect cortical connectivity in Parkinson's disease. *Neuroimage* **158**, 332–345 (2017).
16. T. A. Dembek, J. Roediger, A. Horn, P. Reker, C. Oehrn, H. S. Dafsari, N. Li, A. A. Kühn, G. R. Fink, V. Visser-Vandewalle, M. T. Barbe, L. Timmermann, Probabilistic sweet spots predict motor outcome for deep brain stimulation in Parkinson disease. *Ann. Neurol.* **86**, 527–538 (2019).
17. R. Verhagen, L. J. Bour, V. J. J. Odekerken, P. van den Munckhof, P. R. Schuurman, R. M. A. de Bie, Electrode location in a microelectrode recording-based model of the subthalamic nucleus can predict motor improvement after deep brain stimulation for Parkinson's disease. *Brain Sci.* **9**, 51 (2019).
18. N. Rajamani, H. Friedrich, K. Butenko, T. Dembek, F. Lange, P. Navrátil, P. Zvarova, B. Hollunder, R. M. A. de Bie, V. J. J. Odekerken, J. Volkmann, X. Xu, Z. Ling, C. Yao, P. Ritter, W. J. Neumann, G. P. Skandalakis, S. Komaitis, A. Kalyvas, C. Koutsarnakis, G. Stranjalis, M. Barbe, V. Milanese, M. D. Fox, A. A. Kühn, E. Middlebrooks, N. Li, M. Reich, C. Neudorfer, A. Horn, Deep brain stimulation of symptom-specific networks in Parkinson's disease. *Nat. Commun.* **15**, 4662 (2024).
19. P. Krack, R. Martinez-Fernandez, M. Del Alamo, J. A. Obeso, Current applications and limitations of surgical treatments for movement disorders. *Mov. Disord.* **32**, 36–52 (2017).
20. R. C. Helmich, The cerebral basis of Parkinsonian tremor: A network perspective. *Mov. Disord.* **33**, 219–231 (2018).
21. W. J. Neumann, L. A. Steiner, L. Milosevic, Neurophysiological mechanisms of deep brain stimulation across spatiotemporal resolutions. *Brain* **146**, 4456–4468 (2023).
22. T. Wichmann, H. Bergman, M. R. DeLong, The primate subthalamic nucleus. III. Changes in motor behavior and neuronal activity in the internal pallidum induced by subthalamic inactivation in the MPTP model of parkinsonism. *J. Neurophysiol.* **72**, 521–530 (1994).
23. J. Guridi, M. R. Luquin, M. T. Herrero, J. A. Obeso, The subthalamic nucleus: A possible target for stereotaxic surgery in Parkinson's disease. *Mov. Disord.* **8**, 421–429 (1993).
24. E. Bates, S. M. Wilson, A. P. Saygin, F. Dick, M. I. Sereno, R. T. Knight, N. F. Dronkers, Voxel-based lesion-symptom mapping. *Nat. Neurosci.* **6**, 448–450 (2003).
25. R. Martinez-Fernandez, R. Rodriguez-Rojas, M. Del Álamo, F. Hernandez-Fernandez, J. A. Pineda-Pardo, M. Dileone, F. Alonso-Frech, G. Foffani, I. Obeso, C. Gasca-Salas, E. de Luis-Pastor, L. Vela, J. A. Obeso, Focused ultrasound subthalamotomy in patients with asymmetric Parkinson's disease: A pilot study. *Lancet Neurol.* **17**, 54–63 (2018).
26. R. Martínez-Fernández, J. U. Máñez-Miró, R. Rodríguez-Rojas, M. Del Álamo, B. B. Shah, F. Hernández-Fernández, J. A. Pineda-Pardo, M. H. G. Monje, B. Fernández-Rodríguez, S. A. Sperling, D. Mata-Marín, P. Guida, F. Alonso-Frech, I. Obeso, C. Gasca-Salas, L. Vela-Desojo, W. J. Elias, J. A. Obeso, Randomized trial of focused ultrasound subthalamotomy for Parkinson's disease. *N. Engl. J. Med.* **383**, 2501–2513 (2020).
27. R. Martínez Fernández, E. Natera Villalba, R. Rodríguez-Rojas, M. Del Álamo, J. A. Pineda-Pardo, I. Obeso, D. Mata-Marín, P. Guida, T. Jimenez-Castellanos, D. Pérez-Bueno, A. Duque, J. U. Máñez Miró, C. Gasca-Salas, M. Matarazzo, J. A. Obeso, Unilateral focused ultrasound subthalamotomy in early Parkinson's disease: A pilot study. *J. Neurol. Neurosurg. Psychiatry* **95**, 206–213 (2024).
28. M. A. Mayka, D. M. Corcos, S. E. Leurgans, D. E. Vaillancourt, Three-dimensional locations and boundaries of motor and premotor cortices as defined by functional brain imaging: A meta-analysis. *Neuroimage* **31**, 1453–1474 (2006).
29. F. C. Yeh, Population-based tract-to-region connectome of the human brain and its hierarchical topology. *Nat. Commun.* **13**, 4933 (2022).
30. W. Penfield, B. Milner, Memory deficit produced by bilateral lesions in the hippocampal zone. *AMA Arch. Neurol. Psychiatry* **79**, 475–497 (1958).
31. J. Joutsa, N. Lipsman, A. Horn, G. R. Cosgrove, M. D. Fox, The return of the lesion for localization and therapy. *Brain* **146**, 3146–3155 (2023).
32. P. Cintas, M. Simonetta-Moreau, F. Ory, C. Brefel-Courbon, N. Fabre, P. Chaynes, J. Sabatier, J. C. Sol, O. Rascol, I. Berry, Y. Lazorthes, Deep brain stimulation for Parkinson's disease: Correlation between intraoperative subthalamic nucleus neurophysiology and most effective contacts. *Stereotact. Funct. Neurosurg.* **80**, 108–113 (2003).
33. B. Hollunder, J. L. Ostrem, I. A. Sahin, N. Rajamani, S. Oxenford, K. Butenko, C. Neudorfer, P. Reinhardt, P. Zvarova, M. Polosan, H. Akram, M. Vissani, C. Zhang, B. Sun, P. Navratil, M. M. Reich, J. Volkmann, F. C. Yeh, J. C. Baldermann, T. A. Dembek, V. Visser-Vandewalle, E. J. L. Alho, P. R. Franceschini, P. Nanda, C. Finke, A. A. Kühn, D. D. Dougherty, R. M. Richardson, H. Bergman, M. R. DeLong, A. Mazzoni, L. M. Romito, H. Tyagi, L. Zrinzo, E. M. Joyce, S. Chabardes, P. A. Starr, N. Li, A. Horn, Mapping dysfunctional circuits in the frontal cortex using deep brain stimulation. *Nat. Neurosci.* **27**, 573–586 (2024).
34. G. E. Alexander, M. R. DeLong, P. L. Strick, Parallel organization of functionally segregated circuits linking basal ganglia and cortex. *Annu. Rev. Neurosci.* **9**, 357–381 (1986).
35. A. Nambu, H. Tokuno, M. Inase, M. Takada, Corticosubthalamic input zones from forelimb representations of the dorsal and ventral divisions of the premotor cortex in the macaque monkey: Comparison with the input zones from the primary motor cortex and the supplementary motor area. *Neurosci. Lett.* **239**, 13–16 (1997).
36. M. Takada, H. Tokuno, A. Nambu, M. Inase, Corticostriatal projections from the somatic motor areas of the frontal cortex in the macaque monkey: Segregation versus overlap of input zones from the primary motor cortex, the supplementary motor area, and the premotor cortex. *Exp. Brain Res.* **120**, 114–128 (1998).
37. S. Rahimpour, S. Rajkumar, M. Hallett, The supplementary motor complex in Parkinson's disease. *J. Mov. Disord.* **15**, 21–32 (2022).
38. E. D. Playford, I. H. Jenkins, R. E. Passingham, J. Nutt, R. S. Frackowiak, D. J. Brooks, Impaired mesial frontal and putamen activation in Parkinson's disease: A positron emission tomography study. *Ann. Neurol.* **32**, 151–161 (1992).
39. U. Sabatini, K. Boulanouar, N. Fabre, F. Martin, C. Carel, C. Colonnese, L. Bozzao, I. Berry, J. L. Montastruc, F. Chollet, O. Rascol, Cortical motor reorganization in akinetic patients with Parkinson's disease: A functional MRI study. *Brain* **123**, 394–403 (2000).
40. T. Wu, M. Hallett, A functional MRI study of automatic movements in patients with Parkinson's disease. *Brain* **128**, 2250–2259 (2005).
41. G. E. Alexander, M. D. Crutcher, Preparation for movement: Neural representations of intended direction in three motor areas of the monkey. *J. Neurophysiol.* **64**, 133–150 (1990).
42. M. Jahanshahi, I. H. Jenkins, R. G. Brown, C. D. Marsden, R. E. Passingham, D. J. Brooks, Self-initiated versus externally triggered movements. I. An investigation using measurement of regional cerebral blood flow with PET and movement-related potentials in normal and Parkinson's disease subjects. *Brain* **118**, 913–933 (1995).
43. T. Ninomiya, K. I. Inoue, E. Hoshi, M. Takada, Layer specificity of inputs from supplementary motor area and dorsal premotor cortex to primary motor cortex in macaque monkeys. *Sci. Rep.* **9**, 18230 (2019).
44. M. Bologna, G. Paparella, A. Fasano, M. Hallett, A. Berardelli, Evolving concepts on bradykinesia. *Brain* **143**, 727–750 (2020).
45. A. Nambu, S. Chiken, H. Sano, N. Hatanaka, J. A. Obeso, Dynamic activity model of movement disorders: The fundamental role of the hyperdirect pathway. *Mov. Disord.* **38**, 2145–2150 (2023).
46. R. Chen, A. Berardelli, A. Bhattacharya, M. Bologna, K. S. Chen, A. Fasano, R. C. Helmich, W. D. Hutchison, N. Kamble, A. A. Kühn, A. Macerollo, W.-J. Neumann, P. K. Pal, G. Paparella, A. Suppa, K. Udupa, Clinical neurophysiology of Parkinson's disease and parkinsonism. *Clin. Neurophysiol. Pract.* **7**, 201–227 (2022).
47. N. Baradaran, S. N. Tan, A. Liu, A. Ashoori, S. J. Palmer, Z. J. Wang, M. M. K. Oishi, M. J. McKeown, Parkinson's disease rigidity: Relation to brain connectivity and motor performance. *Front. Neurol.* **4**, 67 (2013).
48. H. T. Benamer, W. H. Oertel, J. Patterson, D. M. Hadley, O. Pogarell, H. Höffken, A. Gerstner, D. G. Grosset, Prospective study of presynaptic dopaminergic imaging in patients with mild Parkinsonism and tremor disorders: Part 1. Baseline and 3-month observations. *Mov. Disord.* **18**, 977–984 (2003).
49. S. A. Shimamoto, E. S. Ryapolova-Webb, J. L. Ostrem, N. B. Galifianakis, K. J. Miller, P. A. Starr, Subthalamic nucleus neurons are synchronized to primary motor cortex local field potentials in Parkinson's disease. *J. Neurosci.* **33**, 7220–7233 (2013).
50. V. Raos, G. Franchi, V. Gallese, L. Fogassi, Somatotopic organization of the lateral part of area F2 (dorsal premotor cortex) of the macaque monkey. *J. Neurophysiol.* **89**, 1503–1518 (2003).
51. D. Akkal, R. P. Dum, P. L. Strick, Supplementary motor area and presupplementary motor area: Targets of basal ganglia and cerebellar output. *J. Neurosci.* **27**, 10659–10673 (2007).
52. A. C. Bostan, R. P. Dum, P. L. Strick, Cerebellar networks with the cerebral cortex and basal ganglia. *Trends Cogn. Sci.* **17**, 241–254 (2013).
53. H. Mure, S. Hirano, C. C. Tang, I. U. Isaias, A. Antonini, Y. Ma, V. Dhawan, D. Eidelberg, Parkinson's disease tremor-related metabolic network: Characterization, progression, and treatment effects. *Neuroimage* **54**, 1244–1253 (2011).
54. A. Quartarone, A. Cacciola, D. Milardi, M. F. Ghilardi, A. Calamuneri, G. Chillemi, G. Anastasi, J. Rothwell, New insights into cortico-basal-cerebellar connectome: Clinical and physiological considerations. *Brain* **143**, 396–406 (2020).
55. A. C. Bostan, R. P. Dum, P. L. Strick, The basal ganglia communicate with the cerebellum. *Proc. Natl. Acad. Sci. U.S.A.* **107**, 8452–8456 (2010).
56. R. C. Helmich, M. J. Janssen, W. J. Oyen, B. R. Bloem, I. Toni, Pallidal dysfunction drives a cerebellothalamic circuit into Parkinson tremor. *Ann. Neurol.* **69**, 269–281 (2011).
57. V. A. Coenen, B. Sajonz, T. Prokop, M. Reisert, T. Piroth, H. Urbach, C. Jenkner, P. C. Reinacher, The dentato-rubro-thalamic tract as the potential common deep brain stimulation target for tremor of various origin: An observational case series. *Acta Neurochir.* **18**, 130–114 (2020).

58. Y. Smith, M. D. Bevan, E. Shink, J. P. Bolam, Microcircuitry of the direct and indirect pathways of the basal ganglia. *Neuroscience* **86**, 353–387 (1998).
59. D. Plenz, S. T. Kital, A basal ganglia pacemaker formed by the subthalamic nucleus and external globus pallidus. *Nature* **400**, 677–682 (1999).
60. J. A. Obeso, M. C. Rodríguez-Oroz, M. Rodríguez, J. L. Lanciego, J. Artieda, N. Gonzalo, C. W. Olanow, Pathophysiology of the basal ganglia in Parkinson's disease. *Trends Neurosci.* **23**, S8–S19 (2000).
61. S. A. Wilson, The Croonian Lectures on some disorders of motility and of muscle tone, with special reference to the corpus striatum. *Lancet* **206**, 215–219 (1925).
62. C. D. Marsden, J. A. Obeso, The functions of the basal ganglia and the paradox of stereotaxic surgery in Parkinson's disease. *Brain* **117**, 877–897 (1994).
63. L. Alvarez, R. Macias, N. Pavón, G. López, M. C. Rodríguez-Oroz, R. Rodríguez, M. Alvarez, I. Pedroso, J. Teijeiro, R. Fernández, E. Casabona, S. Salazar, C. Maragoto, M. Carballo, I. García-Maeso, J. Guridi, J. L. Juncos, M. R. DeLong, J. A. Obeso, Therapeutic efficacy of unilateral subthalamotomy in Parkinson's disease: Results in 89 patients followed for up to 36 months. *J. Neurol. Neurosurg. Psychiatry* **80**, 979–985 (2009).
64. R. Rodriguez-Rojas, M. Carballo-Barreda, L. Alvarez, J. Guridi, N. Pavon, I. Garcia-Maeso, R. Macias, M. C. Rodriguez-Oroz, J. A. Obeso, Subthalamotomy for Parkinson's disease: Clinical outcome and topography of lesions. *J. Neurol. Neurosurg. Psychiatry* **89**, 572–578 (2018).
65. E. Brunner, U. Munzel, The nonparametric Behrens-Fisher problem: Asymptotic theory and a small-sample approximation. *Biom. J.* **42**, 17–25 (2000).
66. C. Rorden, L. Bonilha, T. E. Nichols, Rank-order versus mean based statistics for neuroimaging. *Neuroimage* **35**, 1531–1537 (2007).
67. T. A. Dembek, M. T. Barbe, M. Åström, V. Visser-Vandewalle, G. R. Fink, L. Timmermann, Probabilistic mapping of deep brain stimulation effects in essential tremor. *Neuroimage Clin.* **13**, 164–173 (2016).
68. M. Wintermark, J. Druzgal, D. S. Huss, M. A. Khaled, S. Monteith, P. Raghavan, T. Huerta, L. C. Schweickert, B. Burkholder, J. J. Loomba, E. Zadicario, Y. Qiao, B. Shah, J. Snell, M. Eames, R. Frysinger, N. Kassell, W. J. Elias, Imaging findings in MR imaging-guided focused ultrasound treatment for patients with essential tremor. *AJNR Am. J. Neuroradiol.* **35**, 891–896 (2014).
69. A. Klein, J. Andersson, B. A. Ardekani, J. Ashburner, B. Avants, M. C. Chiang, G. E. Christensen, D. L. Collins, J. Gee, P. Hellier, J. H. Song, M. Jenkinson, C. Lepage, D. Rueckert, P. Thompson, T. Vercauteren, R. P. Woods, J. J. Mann, R. V. Parsey, Evaluation of 14 nonlinear deformation algorithms applied to human brain MRI registration. *Neuroimage* **46**, 786–802 (2009).
70. Q. Wang, H. Akram, M. Muthuraman, G. Gonzalez-Escamilla, S. A. Sheth, S. Oxenford, F. C. Yeh, S. Groppa, N. Vanegas-Arroyave, L. Zrinzo, N. Li, A. Kühn, A. Horn, Normative vs. patient-specific brain connectivity in deep brain stimulation. *Neuroimage* **224**, 117307 (2021).
71. C. G. Goetz, B. C. Tilley, S. R. Shaftman, G. T. Stebbins, S. Fahn, P. Martinez-Martin, W. Poewe, C. Sampaio, M. B. Stern, R. Dodel, B. Dubois, R. Holloway, J. Jankovic, J. Kulisevsky, A. E. Lang, A. Lees, S. Leurgans, P. A. LeWitt, D. Nyenhuis, C. W. Olanow, O. Rascol, A. Schrag, J. A. Teresi, J. J. van Hilten, N. LaPelle, Movement Disorder Society UPDRS Revision Task Force, Movement Disorder Society-sponsored revision of the Unified Parkinson's Disease Rating Scale (MDS-UPDRS): Scale presentation and clinimetric testing results. *Mov. Disord.* **23**, 2129–2170 (2008).
72. J. Ashburner, A fast diffeomorphic image registration algorithm. *Neuroimage* **38**, 95–113 (2007).
73. T. A. Dembek, J. C. Baldermann, J. N. Petry-Schmelzer, H. Jergas, H. Treuer, V. Visser-Vandewalle, H. S. Dafsari, M. T. Barbe, Sweetspot mapping in deep brain stimulation: Strengths and limitations of current approaches. *Neuromodulation* **25**, 877–887 (2022).
74. J. Medina, D. Y. Kimberg, A. Chatterjee, H. Coslett, Inappropriate usage of the Brunner-Munzel test in recent voxel-based lesion-symptom mapping studies. *Neuropsychologia* **48**, 341–343 (2010).
75. Y. Iturria-Medina, E. J. Canales-Rodríguez, L. Melie-García, P. A. Valdés-Hernández, E. Martínez-Montes, Y. Alemán-Gómez, J. M. Sánchez-Bornot, Characterizing brain anatomical connections using diffusion weighted MRI and graph theory. *Neuroimage* **36**, 645–660 (2007).
76. B. L. Edlow, A. Mareyam, A. Horn, J. R. Polimeni, T. Witzel, M. D. Tisdall, J. C. Augustinack, J. P. Stockmann, B. R. Diamond, A. Stevens, L. S. Tirrell, R. D. Folkerth, L. L. Wald, B. Fischl, A. van der Kouwe, 7 Tesla MRI of the ex vivo human brain at 100 micron resolution. *Sci. Data* **6**, 244 (2019).
77. A. J. Rico, P. Barroso-Chinea, L. Conte-Perales, E. Roda, V. Gómez-Bautista, M. Gendive, J. A. Obeso, J. Lanciego, A direct projection from the subthalamic nucleus to the ventral thalamus in monkeys. *Neurobiol. Dis.* **39**, 381–392 (2010).
78. S. Ewert, P. Plettig, N. Li, M. M. Chakravarty, D. L. Collins, T. M. Herrington, A. A. Kühn, A. Horn, Toward defining deep brain stimulation targets in MNI space: A subcortical atlas based on multimodal MRI, histology and structural connectivity. *Neuroimage* **170**, 271–282 (2018).
79. G. Schaltenbrand, W. Wahren, *Atlas of Stereotaxy of the Human Brain* (Thieme, 1977).

Acknowledgments: We are grateful to A. Horn (Harvard University) for insightful comments and suggestions and L. H. Phillips (Charlottesville, VA) for copy editing and repeatedly revising the manuscript. We like to recognize the influence and inspiration of M. DeLong (1938 to 2024) whose career will continue to inspire us in the years to come. **Funding:** The study was partially supported by the Fundación de Investigación HM Hospitales (Madrid). J.A.O. research in this area is supported by the Plan Nacional de Investigación (PID2019-111045RB-I00), Ministry of Science and Education, Spain, Fundación MAPFRE, and the Focused Ultrasound Foundation (Virginia, United States). The supporting party had no role in data acquisition, analysis, or interpretation. The corresponding author confirms that he had full access to all the data in the study and had final responsibility for the decision to submit for publication. **Author contributions:** Conceptualization, methodology, software, validation, formal analysis, investigation, data curation, visualization, writing—original draft, and writing—review and editing: R.R.-R. Conceptualization, methodology, validation, formal analysis, investigation, resources, data curation, visualization, writing—original draft, writing—review and editing, and project administration: J.U.M.-M. Conceptualization, methodology, software, formal analysis, investigation, and writing—review and editing: J.A.P.-P. Conceptualization, investigation, data curation, and writing—review and editing: M.d.Á. Conceptualization, methodology, investigation, resources, writing—review and editing, and project administration: R.M.-F. Conceptualization, methodology, investigation, resources, writing—original draft, writing—review and editing, validation, visualization, supervision, project administration, and funding acquisition: J.A.O. **Competing interests:** R.R.-R. has received speaker honoraria from Insightec and Zambon. J.U.M.-M. has received speaker honoraria from Insightec, Bial, and Zambon and reimbursement of travel expenses to attend scientific conferences from Insightec, Bial, and Lundbeck. M.d.Á. has received speaker honoraria from Insightec and Boston Scientific and reimbursement of travel expenses to attend scientific conferences from Boston Scientific and Medtronic. R.M.-F. has received speaker honoraria from Insightec, Bial, Zambon, and Boston Scientific and reimbursement of travel expenses to attend scientific conferences from Insightec and BIAL. J.A.O. has received honoraria for lecturing and reimbursement of travel expenses to attend scientific meetings by Insightec and honoraria for attending advisory boards of Biogen, Insightec, and Bial. The authors declare that they have no other competing interests. **Data and materials availability:** All data needed to evaluate the conclusions in the paper are present in the paper and/or the Supplementary Materials. Lesion's probabilistic maps and sign-related sweet spots are available in the EU Open Research Repository (https://zenodo.org/records/13889651). The HCP-1065 diffusion template used to reconstruct the track fibers can be openly accessed via the DSI-Studio (https://brain.labsolver.org/hcp_template.html; fiber orientation maps at a 1-mm resolution). Toolbox used for nonparametric voxel-based lesion-symptom mapping is openly available with the MRIcron software (https://nitrc.org/projects/mricron).

Submitted 29 July 2024
Accepted 23 October 2024
Published 22 November 2024
10.1126/sciadv.adr9891